Electronic and phonon properties of BX(110) (X=P, As, and Sb) and BeY(110) (Y=S, Se, and Te) surfaces

S. Bağci,[1] S. Duman,[1] H. M. Tütüncü,[1] and G. P. Srivastava[2]
[1]*Fen-Edebiyat Fakültesi, Fizik Bölümü, Sakarya Üniversitesi, 54187 Adapazarı, Turkey*
[2]*School of Physics, University of Exeter, Stocker Road, Exeter EX4 4QL, United Kingdom*
(Received 16 December 2008; revised manuscript received 16 February 2009; published 30 March 2009)

We have employed the *ab initio* plane-wave pseudopotential method, within a local-density approximation of the density-functional theory, and a linear-response approach, to investigate structural, electronic and phonon properties of boron compounds (BP, BAs, and BSb). The calculated structural and electronic results for these semiconductors are in good agreement with available theoretical and experimental studies. In addition to these bulk studies, the elastic constants of zinc-blende boron compounds and beryllium chalcogenides have been calculated using the volume-conserving tetragonal and monoclinic strains. In particular, a good agreement has been observed between our calculated elastic constants and their experimental values for BP semiconductor. Furthermore, we have made theoretical investigations of the atomic geometry, electronic structure, and lattice dynamics of the (110) surface of boron compounds and beryllium chalcogenides. The structural properties for these surfaces are compared with previous structural results obtained for other III-V(110) and II-VI(110) surfaces in detail. Our results clearly indicate that the electronic structure for these surfaces is semiconductor due to separation between a highest occupied surface state and lowest unoccupied surface state. The origins of various phonon modes on these surfaces are discussed and their variations for different compounds are analyzed in terms of the reduced mass and total mass differences. Moreover, surface phonon modes on these surfaces are compared with the corresponding phonon modes on other III-V(110) and II-VI(110) surfaces. From this comparison, some differences are observed and they are explained according to mass differences and ionicity factor.

DOI: 10.1103/PhysRevB.79.125326 PACS number(s): 62.20.de, 63.20.dk, 68.35.B−, 68.35.Ja

I. INTRODUCTION

III-V and II-VI semiconductors have attracted the attention of the physicists due to their wide technological applications. However, zinc-blende boron compound and beryllium chalcogenides have received considerably less attention than the elemental group III-V (such as GaAs, InP, and AlSb) and elemental group II-VI (such as ZnS, ZnSe, and ZnTe) materials. On the other hand, these semiconductors have a number of remarkable properties which set them apart from other III-V and make them particularity worthy of study. First, they are potential good choice for proactive coatings due to their hardness, high melting point, high thermal conductivity, and large modulus.[1] Second, they are promising semiconductors for blue and ultraviolet-wavelength optics and high-temperature electronics due to their large band gaps and low dielectric constants.[2] In order to use them in optoelectronic devices healthy, experimental, and theoretical research on the structural, elastic, electronic, and vibrational properties is desirable. As a result of this reality, several studies have been done on the above properties of these materials. On the theoretical side, several theoretical calculations have been made in order to obtain structural, elastic, and electronic properties of these materials.[3–17] Despite several theoretical works on these materials, less attention has been paid on the experimental side.[18–23] This can be related to difficulty in growing single crystals or good quality epitaxial layers. Some experimental results are available for structural and el ctronic properties of these materials[18,20–23] while experimental elastic constants results are only reported for BP.[19] In addition to these experimental results, experimental investigations of zone-center phonon modes in BP have been made using Raman spectroscopy.[24] Recently, we have presented the full phonon spectrum and density of states for BeS, BeSe, and BeTe by employing a linear-response approach based on the density-functional theory[25] while several theoretical groups have studied phonons in boron compounds.[26–31]

Despite the wealth of theoretical works presented in recent years on bulk properties of these semiconductors, their surface properties are totally ignored in the literature. It is well known that microscopic investigations of atomic geometry, electronic states, and phonon modes on semiconductor surfaces are very important in view of their increasing role in electronic and optical devices. Thus, we have studied structural and electronic properties of boron compounds and beryllium chalcogenides by using plane-wave pseudopotential method within density-functional theory. The clear relaxation picture of these surfaces is presented and compared with other III-V(110)[32–35] and II-VI(110) surfaces.[36] The surface electronic states on these surfaces are identified by comparing surface electronic and projected bulk electronic spectrum. In addition to structural and electronic properties, surface phonons on these surfaces have been identified using a linear-response approach based on density-functional theory. Phonon dispersion curves of these surfaces are compared with the corresponding phonon dispersion curves for other III-V surfaces.[33–35] From this comparison, some important differences have been observed and discussed. Moreover, we have presented the density of states for both the slab geometry and the bulk together. Thus, we have identified and discussed phonon modes related to surface atomic vibrations.

II. THEORY

Our calculations are made using the plane-wave pseudopotential approach within the framework of the density-functional theory. Electronic exchange and correlation energies are taken into account within the local-density approximation (LDA) using a standard form for the exchange-correlation potential.[37,38] To describe the electron-ion interaction, we use the norm-conserving pseudopotential.[39] The electronic wave functions are expanded in plane waves up to a maximal cutoff energy of 40 Ry. Self-consistent solutions to the Kohn-Sham equations[40] were obtained by employing a set of ten special **k** points. In our surface calculations, once the lattice parameter was determined for each semiconductor, a model for the (110) surface has been constructed using a slab model approach. In this approach one uses a unit cell which is repeated periodically in two dimensions while it has a finite extent in the third one. In order to use the plane-wave basis set which is periodic in nature the corresponding slab is repeated in the third direction with slab separated by a sufficiently wide vacuum region. Our supercell was considered to contain 30 atoms located in a slab of 15 atomic layers and a vacuum region along the surface normal equivalent of five atomic layers. For the **k**-point sampling, nine special points have been used in the irreducible part of the surface Brillouin zone. The equilibrium positions of atoms in the unit cell are calculated by minimizing the total energy with the help of the Hellmann-Feynman forces, starting the atomic relaxation from the ideal positions derived from the symmetry of the bulk. Each atom is allowed to move with exception of the central-layer atoms. The equilibrium positions are determined with numerical uncertainty of less than 0.01 Å when all forces are smaller than 0.1 mRy/au.

A cubic crystal has three independent elastic constants:C_{11}, C_{12}, and C_{44}. The straightforward manner of obtaining these constants is to calculate the total energy difference between an unstrained medium and a distorted medium at constant volume. We have used the volume-conserving tetragonal and monoclinic strains for $C_{11}-C_{12}$ and C_{44}, respectively.[41,42] In order to obtain C_{11} and C_{12} separately, the relationship between these elastic constants and bulk modulus

$$B = \frac{1}{3}(C_{11} + 2C_{12}) \tag{1}$$

is also used.

Phonon properties of bulk semiconductors have been studied by means of the density-functional perturbation theory of Baroni *et al.*[43] Within this approach, second derivatives of the total energy were calculated to obtain the dynamical matrix. The response of the electrons is calculated iteratively, until self-consistency is achieved between the variation in the charge density and the screened perturbing potential. In order to generate the force constants matrices for bulk semiconductors and carry out the inverse Fourier transformation, we used **q** points on a $4\times4\times4$ mesh. For surface phonon calculations, we calculated nine dynamical matrices corresponding to a $4\times4\times1$ **q**-point mesh within the irreducible segment of the surface Brillouin zone. Then, two-dimensional Fourier interpolation was used to calculate phonons for any chosen **q** points.

TABLE I. Lattice constant a, bulk modulus B, the pressure derivative of bulk modulus B' and macroscopic dielectric constant ε_∞ for BP, BAs and BSb are compared with other theoretical and experimental data. PM in parenthesis means theoretical phenomenological model.

	a (Å)	B (Mbar)	B'	ε_∞
BP (Present work)	4.50	1.678	3.55	9.43
Theory (LDA) (Ref. 4)	4.47	1.720		
Theory (LDA) (Ref. 12)	4.50	1.760	3.68	
Theory (LDA) (Ref. 29)	4.46	1.760	4.00	9.37
Theory (LDA) (Ref. 8)	4.47	1.720		
Theory (PM) (Ref. 17)	4.55	1.617	3.10	
Experimental (Ref. 18)	4.53	1.720		9.60
Experimental (Ref. 19)		1.730		
BAs (Present work)	4.74	1.473	4.24	9.60
Theory (LDA) (Ref. 12)	4.74	1.520	3.65	
Theory (LDA) (Ref. 29)	4.73	1.470	3.00	9.65
Theory (LDA) (Ref. 8)	4.72	1.440	4.00	
Theory (LDA) (Ref. 13)	4.72	1.480		9.80
Theory (PM) (Ref. 17)	4.81	1.324	3.20	
Experimental (Ref. 18)	4.77			
BSb (Present work)	5.24	1.029	3.84	11.46
Theory (LDA) (Ref. 12)	5.20	1.160	4.16	
Theory (LDA) (Ref. 29)	5.20	1.090	4.00	11.30
Theory (LDA) (Ref. 8)	5.16	1.080	4.03	
Theory (PM) (Ref. 17)	5.22	1.002	4.70	

III. RESULTS

A. Bulk properties

1. Structural and elastic properties

The structural properties of BP, Bas, and BSb are investigated by calculating the total energy for the unit cell as a function of the lattice parameter a. The calculated total energies were fitted to the Murnaghan's equation of state[44] in order to obtain the ground-state properties such as the equilibrium lattice constant, the bulk modulus (B), and its pressure derivative (B'). Table I presents our results of these properties for BP, BAs, and BSb, in comparison with available experimental[18,19] and theoretical[4,8,12,13,17,29] results. First, we can see that the calculated lattice constants for BP and BAs are in good agreement with the other theoretical[4,8,12] and experimental results,[18,19] within LDA error. Unfortunately, we have not able to find any experimental data for the lattice constant of BSb but the calculated value is very close with the available theoretical values[8,12,17,29] an error of 1.6%. Since we will focus next on the elastic constants, we pay particular attention to bulk modulus (B),

TABLE II. Calculated elastic constants (in unit of Mbar) for zinc-blende phase of BP, BAs, BSb, BeS, BeSe, and BeTe. The obtained results are also compared with previous theoretical and experimental results. GGA means generalized gradient approximation.

	Source	BP	BAs	BSb	BeS	BeSe	BeTe
	This result	3.41	2.91	1.93	1.60	1.35	1.03
	LDA (Ref. 12)	3.57	2.95	2.23			
	LDA (Ref. 11)	3.59	2.91	2.05			
C_{11}	LDA (Ref. 13)		2.86				
	LDA (Ref. 16)				1.69	1.37	0.98
	LDA (Ref. 5)				1.84	1.49	1.11
	LDA (Ref. 10)				1.87		
	GGA (Ref. 28)	3.56					
	Experimental (Ref. 19)	3.15					
	This result	0.80	0.76	0.58	0.60	0.53	0.39
	LDA (Ref. 12)	0.87	0.78	0.62			
	LDA (Ref. 11)	0.81	0.73	0.63			
C_{12}	LDA (Ref. 13)		0.67				
	LDA (Ref. 16)				0.68	0.58	0.46
	LDA (Ref. 5)				0.75	0.59	0.43
	LDA (Ref. 10)				0.75		
	GGA (Ref. 28)	0.68					
	Experimental (Ref. 19)	1.00					
	This result	1.90	1.58	1.02	0.85	0.69	0.53
	LDA (Ref. 12)	1.50	1.77	1.40			
	LDA (Ref. 11)	1.97	1.58	1.12			
C_{44}	LDA (Ref. 13)		1.48				
	LDA (Ref. 16)				1.06	0.90	0.68
	LDA (Ref. 5)				0.99	0.81	0.60
	LDA (Ref. 10)				0.82		
	GGA (Ref. 28)	2.05					
	Experimental (Ref. 19)	1.60					

which is essentially an elastic constant. Owing to the smaller volume of BP, the calculated bulk modulus is larger than those of either BAs or BSb. We see in Table I that we obtain rather good agreement between our values and experimental data[18,19] (or previous theoretical results[4,8,12,13,17,29]). The calculated optical dielectric constant results of 9.43, 9.60, and 11.46 for BP, BAs, and BSb compare well with their previous LDA values of 9.37, 9.65, and 11.30, respectively.[29] Moreover, good agreement has been observed between our theoretical calculations and experimental data[18] for the optical dielectric constant of BP.

In Table II, the calculated and previous theoretical values of the elastic constants for BP, BAs, BSb, BeS, BeSe, and BeTe are listed. They were calculated at the theoretical equilibrium volumes. The requirement of mechanical stability in a cubic crystal leads to the following restrictions on the elastic constants: $C_{11}>0$, $C_{44}>0$, $C_{11}-C_{12}>0$, and $C_{11}+2C_{12}>0$. Our calculated elastic constants in Table II obey these stability conditions, including the fact that C_{12} should be smaller than C_{11}. To the best of our knowledge experimental data[19] are only available for BP. The calculated C_{11} for BP is 8% lower than the experimental value while the discrepancy between our calculated C_{44} and its experimental value[19] is around 20%. When comparing our calculated elastic constants and previous theoretical results[11–13,28] for BX, we see that generally the discrepancy is less than 10% but can reach 27% in the worst cases. These ranges are comparable with previous theoretical studies.[11–13,28] For BeY semiconductors, the agreement between our calculations and previous theoretical calculations[5,10,16] is good. The maximum discrepancy is less than 25% between our elastic constants and their previous theoretical values.[5,10,16] Different from BX semiconductors, the C_{12} and C_{44} values of BeY semiconductors are close to each other. This brings the Cauchy relation ($C_{12}=C_{44}$) in mind. This relation holds true for crystals bound only by central forces. Table II clearly shows that BX semiconductors do not obey this equality due to their covalent character. However, C_{12} and C_{44} values are very close to each other for BeY semiconductors because these semiconductors are less covalent than BX semiconductors.

2. Electronic properties

The electronic band structures of BP, Bas, and BSb calculated with the LDA method are shown in Fig. 1. The band

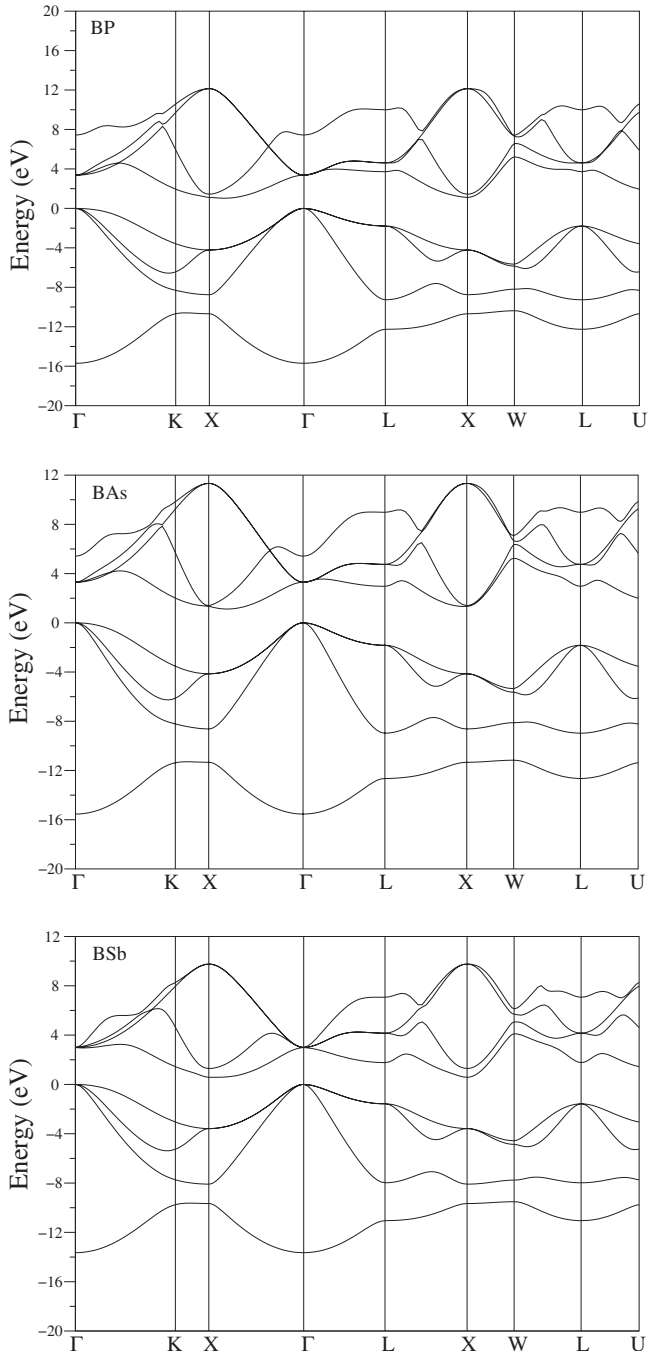

FIG. 1. The electronic band structure for BP, BAs, and BSb.

structures of these semiconductors are very similar to each other. The overall band profiles are found to be same for all the three compounds. The valence-band maximum occurs at the Γ point and the conduction-band minimum is along the Γ-*X* direction close to the *X* point indicating that these materials have an indirect band gap. These results are consistent with the previous experimental[18,20–23] and theoretical[3,6,7,15] findings. The main band features are summarized in Table III together with previous theoretical works[3,6,7,15] as well as experimental data.[18,20–23] Satisfactory agreement is found between our and previous LDA calculations.[3,6,15] It is well known that the application of the LDA results in an underestimation of band gaps in semiconductors. Our results are consistent with this general picture. Indeed, the application of the GW method by Surh *et al.*[3] produces band-gap values of 1.90 eV (an increase of 83% over our LDA result) for BP and 1.60 eV (an increase of 43% over our LDA result) for BAs. Figure 1 shows clearly four occupied valence bands, i.e., eight electrons, with lowest band well separated from other three bands. The lowest band has a parabolic shape along the main symmetry directions of [110], [100], and [111]. In order to clarify the characters of all the bands, the total and partial densities of states (DOS) for BP are shown in Fig. 2. The total valence DOS exhibits three distinct regions that we may call VB1, VB2, and VB3 for the valence bands. VB1 is an isolated band consisting of 3*s*-P, 2*p*-B, and 2*s*-B orbitals. VB2 is a very sharp peak around −8 eV and is primarily composed of electrons from the 3*p* bands of P atom, with some contribution from B 2*s* band electrons. VB3 is dominated by nearly equal contributions of B and P *p* orbitals. Because of the hybridization, this feature distributes in a wide energy range (about 7 eV). As can be seen from Fig. 2, this feature even continues in the conduction bands of BP which are mainly composed of P 3*p* hybridized with B 2*p*. Similar features have been observed for other boron compounds while electronic properties of Be-chalcogenides were clearly discussed in our previous work.[25]

3. Phonons

The results for the phonon dispersion curves of BP, Bas, and BSb semiconductors in the zinc-blende structure are displayed in Fig. 3 along several high symmetry directions together with the corresponding phonon density of states. A striking feature in their phonon dispersion curves is a very small separation between zone-center longitudinal and transverse optical (LO and TO) phonon modes. This picture can be related to the strong covalent character of these semiconductors. As a result, one can say that the covalent bonding in these semiconductors is much stronger than the covalent bonding in other III-V semiconductors[45] such as GaAs, InP, GaP, and InAs. We have calculated the zone-center TO (LO) phonon modes with frequencies 811 cm^{-1} (817 cm^{-1}) for BP, 702 cm^{-1} (706 cm^{-1}) for BAs, and 600 cm^{-1} (612 cm^{-1}) for BSb. The calculated TO and LO values for BP compare very well with experimentally measured value, using Raman spectroscopy, of 799 cm^{-1} (TO) and 829 cm^{-1} (LO), respectively.[24] Another striking feature in their phonon dispersion curves is that the frequency scales for these semiconductors are mainly determined by the masses of the anion species, P, As, and Sb. Yet another striking feature is that the acoustic phonon branches are well separated from the optical ones in all of the three semiconductors. The gap between these branches is larger in BSb and smaller in BP due to the large mass difference between the boron and anions (see also the phonon density of states for these semiconductors). The frequency of this gap is found to be 368 cm^{-1} for BSb, 258 cm^{-1} for BAs, and 135 cm^{-1} for BP. The computed transverse and longitudinal acoustic (TA and LA) branches behave normally in the long-wave limit with steep slopes. In the short-wave limit (close to zone edges of *X* and *L*), TA branch for these semiconductors is nearly flat along the [100] and [111] directions. The first peak in their DOS can be

TABLE III. Electronic band gaps (in units of eV) for bulk electronic spectrum of BP, BAs, and BSb at the high symmetry points and Γ-X.

	Γ-Γ	X-X	L-L	Γ-X	E_{gap}	Val. bandwidth
BP	3.37	5.33	5.51	1.12	1.04	15.71
LDA (Ref. 15)	3.40	5.74	5.73	1.25	1.15	15.60
LDA (Ref. 3)	3.40	5.40	5.40	1.30	1.20	15.50
GW (Ref. 3)	4.40	6.50	6.50	2.00	1.90	16.80
Tight binding (Ref. 7)	4.43	6.38	7.13	1.88	0.94	16.80
EXP (Refs. 18, 20, and 21)	5.00			2.40		16.50
BAs	3.30	5.48	4.79	1.34	1.12	15.54
LDA (Ref. 15)	3.25	5.57	4.84	1.31	1.18	15.31
LDA (Ref. 3)	3.10	5.46	4.40	1.36	1.10	15.50
GW (Ref. 3)	4.20	6.43	5.30	1.93	1.60	16.70
Tight binding (Ref. 7)	2.90	4.47	4.21	1.18	0.30	16.63
EXP (Ref. 22)						16.00
BSb	2.99	4.16	3.34	0.58	0.57	13.65
LDA (Ref. 15)	2.97	4.26	3.98	0.48	0.48	13.40
LDA (Ref. 6)	3.06	4.41	3.73	1.27	0.53	14.35
EXP (Ref. 23)					0.58	

related to the flatness of their TA branch. Finally, different from BAs and BSb, the most remarkable characteristic of the optical branches in BP is that LO and TO branches cross at about $\frac{2\pi}{a}(0.45,0.45,0.45)$. This characteristic is not found in BAs and BSb. Thus, this difference can be linked to the smaller mass difference between B and P atoms. This observation has been made in the theoretical calculation of Talwar *et al.*[27] Our calculated zone-center and zone-edge phonon results for BP are compared with available theoretical[26–29] and experimental[24] results in Table IV. In general our results are in good agreement with previous theoretical calculations.[26–29] However, we note that the crossing between LO and TO branches along the Γ-L direction has not been found in three previous theoretical calculations.[26,28,29]

B. Surface properties

1. Structural properties

A (110) surface of the zinc-blende-type semiconductors is nonpolarized, in which the outermost layer of an ideal (110) surface consists of an equal number of cation and anion atoms. The relaxation of BX(110) and BeY(110) surfaces is well known: the cation-anion chain become tilted with the anions being raised, as shown in Fig. 4. For the relaxed systems, it is found that the surface bond lengths deviate no more than about 4% from their bulk values. The shortening of atomic bond length on the (110) surface of zinc-blende semiconductors has been well documented and clearly indicates that interatomic bonding on semiconductor surfaces is stronger than the corresponding bulk bonding. Moreover, the atoms in the fourth layer are nearly in their ideal bulk positions. Thus, the relaxation can be expressed in terms of the tilt angles of atomic chains in the three outermost layers, as shown in Fig. 4. The relaxations typical of the (110) surface of most zinc-blende semiconductors have been generally interpreted as driven by a loss of sp^3 hybridization toward anion p and cation sp^2-like character. In this relaxation, the dangling bonds of the surface cations are empty while the dangling bonds of the surface anions are fully occupied.

The calculated key structural parameters of the clean relaxed BX(110) and BeY(110) surfaces, defined in Fig. 4, are listed in Table V. The tilt angles (ω) for BP(110), BAs(110), BSb(110), BeS(110), BeSe(110), and BeTe(110) are found to be 24.4°, 26.1°, 26.5°, 26.3°, 28.3°, and 28.8°, respectively. The tilt angles for BeY(110) surfaces are very close to the corresponding tilt angles 30.4° for CdTe(110), 29.6° for ZnTe(110), and 27.1° for ZnS(110) surfaces.[36] As can be seen from Table V, the vertical buckling of the top layer $\Delta_{1,\perp}$ is increased when the surface bond length d_{sb} is increased. Thus, we have plotted $\Delta_{1,\perp}$ against d_{sb} in Fig. 5. This figure shows nearly linear behavior between $\Delta_{1,\perp}$ and d_{sb}. This relationship can be explained in term of Duke's formula $\Delta_{1,\perp} = \frac{a_o}{4}\sin(\omega)$, implying a constant value of ω.

2. Electronic properties

Figure 6 shows the electronic structure of the BP(110) and BeS(110) surfaces along the several symmetry directions of surface Brillouin zone. The general pattern of the electronic structure of these surfaces is similar to that on other III-V(110) and II-VI(110) surfaces.[32–36] It is interesting to note that there are gaps in the projected bulk band structures, in which bulk states are inaccessible. There are four surface states for both surfaces in these gap regions. Three of them are occupied (S^1 to S^3) surface states while the highest of them is the lowest unoccupied (S^4) state. The lowest occupied (S^1) state is derived from the electrons on the surface anion atom for both surfaces. This state is nearly flat for the BeS(110) surface while it has parabolic shape along the

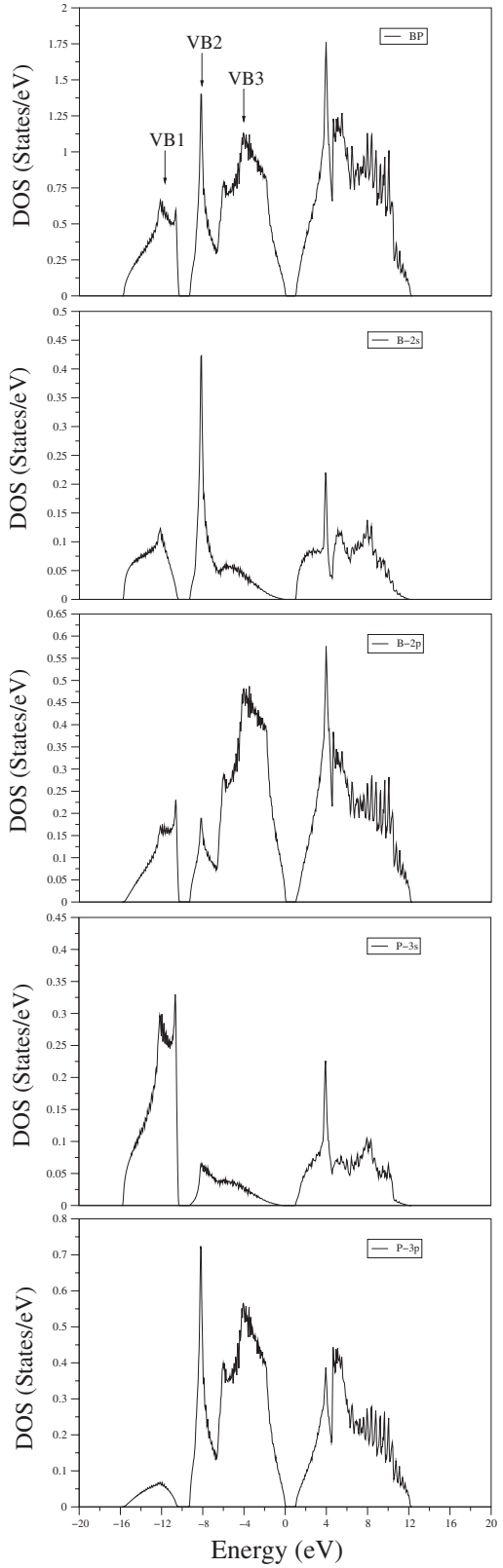

FIG. 2. Total and projected density of states (DOS) for BP.

$\bar{M}$-$\overline{X'}$ and $\bar{\Gamma}$-$\overline{X'}$ directions for the BP(110) surface. This parabolic shape has been observed for other BX(110) surfaces. The second occupied state (S^2) for both surfaces lies in the stomach gap region and shows strong dispersion along the

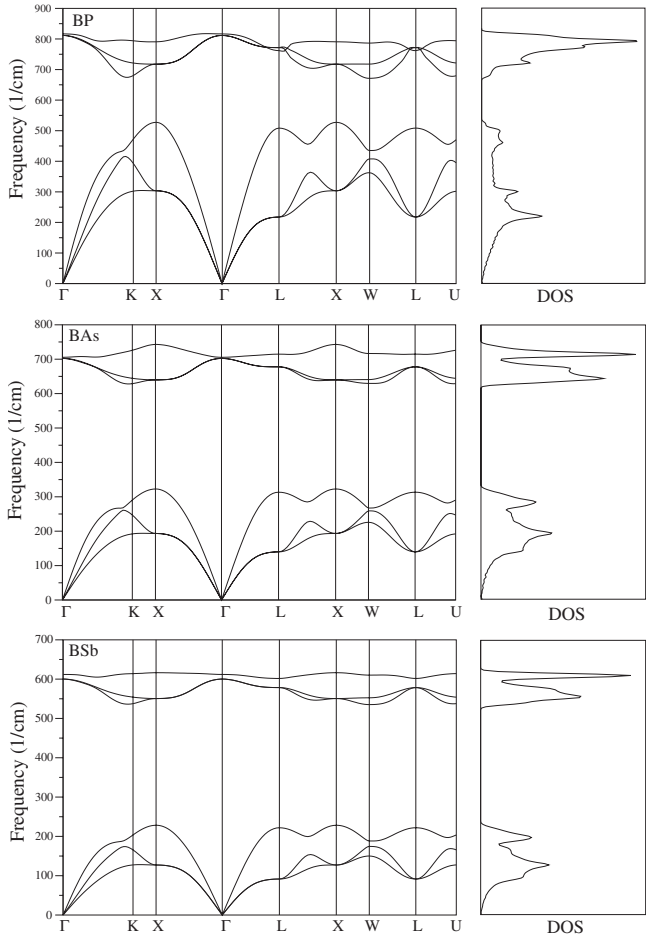

FIG. 3. Theoretical phonon dispersion curves and density of states for BP, BAs, and BSb.

$\bar{M}$-$\overline{X'}$ direction. S^3 is the highest occupied level, and lies rather flat along $\bar{X}$-$\bar{M}$ and $\bar{M}$-$\overline{X'}$ at approximately 1 eV for BP(110) and 0.8 eV for BeS(110) below the top of the bulk valence band. This band is an anion-derived dangling bond state while the S^4 state is related to the empty cation-derived dangling bonds for both surfaces. The splitting between the S^3 and S^4 states is found to be around 1.7 eV for BP(110) and 4.2 eV for BeS(110) at the zone edges of the surface Brillouin zone.

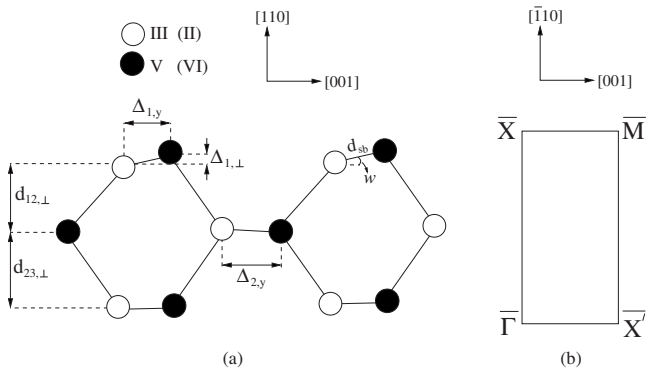

FIG. 4. Schematic representation of the relaxed atomic positions indicating the key structural parameters for the cubic (110) surfaces of III-V and II-VI compounds.

TABLE IV. Phonon frequencies (in cm^{-1}) calculated at the high-symmetry points Γ, X, and L for BP. The results are compared with available experimental and theoretical results.

	Γ_{TO}	Γ_{LO}	X_{TA}	X_{LA}	X_{TO}	X_{LO}	L_{TA}	L_{LA}	L_{TO}	L_{LO}
This work	811	817	303	527	717	790	218	508	772	762
Theory (Ref. 26)	808		306	527	701	800		506		764
Theory (Ref. 27)	800	830	294	502	707	803	243	529	747	727
Theory (Ref. 28)	797	797	318	526	698	781	227	506	752	755
Theory (Ref. 29)	813	838	326	542	729	818	224	516	787	792
Experimental (Ref. 24)	799	829								

3. Surface phonon properties

The surface-phonon dispersions of the BX(110) surfaces are shown in Fig. 7 along the several symmetry directions in the two-dimensional Brillouin zone. The shaded regions are the projection of bulk-phonon bands. Also shown in Fig. 7 are the density of states for both the slab geometry and the bulk. We first briefly discuss the bulk phonon characteristic. We find that there is a trend in the bulk phonon spectrum of the compounds studied here: the acoustic and optical band-edge frequencies, as well as the acoustic-optical band gap, increase as we move along BP, BAs, and BSb. For the BX(110) surfaces, studied here, we have identified, as expected, up to 12 surface modes corresponding to vibrations of atoms in the top two layers. Three of these are surface acoustic modes, and the rest of them are surface optical. Because of the reduced atomic coordination at the surface, the lowest acoustic phonon branch for the BX(110) surfaces (known as Rayleigh mode) may appear as truly localized by falling the bulk continuum at the edges of the surface Brillouin zone. There is a clear peak in the phonon density of states for BX(110) due to the flatness of Rayleigh phonon branch close the zone edges. The energy of this peak is found to be 21 meV for BP(110), 13 meV for BAs(110), and 9 meV for BSb(110). Surface optical modes may appear as truly localized both within the acoustic-optical gap region and above the optical continuum of the bulk spectrum. In the acoustic stomach gap region we find only one localized mode on all the considered BX(110) surfaces. In the acoustic-optical gap region we have identified up to three gap phonon modes on both BAs(110) and BSb(110) while only one phonon mode has been observed for BP(110) in this gap region. The lower gap phonon branch for the BAs(110) and BSb(110) surfaces is nearly flat along all symmetry directions on the surface Brillouin zone. This flatness can be related to the large cation-anion mass difference because a similar observation has made for InP(110) and AlSb(110) surfaces.[33–35] This gap phonon branch leads a small but clear peak at 48 and 40 meV in the phonon density of states on BAs(110) and BSb(110) surfaces, respectively. Due to the nature of optical phonon modes, the energy difference between these peaks can be explained in terms of reduced mass (μ) and lattice constant (a) differences between these materials. Thus, the gap phonon peak on the BAs(110) surface can be calculated from the corresponding peak on the BSb(110) surface following scaling relation:

$$\nu_{\mathrm{gap}}(\mathrm{BAs}) = \sqrt{\frac{\mu^{\mathrm{BSb}}}{\mu^{\mathrm{BAs}}}} \cdot \frac{a^{\mathrm{BSb}}}{a^{\mathrm{BAs}}} \nu_{\mathrm{gap}}(\mathrm{BSb}). \tag{2}$$

From the above equation, the peak due the lower gap phonon mode on BAs(110) is estimated to 45 meV which can be compared with our calculated value of 48 meV. This observation indicates that effective force constants governing the localized gap phonon mode on the (110) surface of BAs and BSb are rather similar. Different from other III-V(110) surfaces,[33–35] the highest surface optical phonon branch on BX(110) surfaces lies well above the bulk continuum. We have also observed clear peaks due to this phonon branch in the phonon density of states for the BX(110) surfaces.

When the wave vector is along the $\bar{\Gamma}$-$\overline{X'}$ axes, there is a mirror reflection symmetry about the plane which contains the surface normal and the wave vector. Thus the vibration is separated in to a saggital-plane (SP) mode which oscillates in the plane and a shear-horizontal (SH) mode whose eigenvector is vertical to the plane. Only SP mode is observable by electron-energy-loss spectroscopy. In particular, vibrations

TABLE V. Calculated structural parameters, defined in Fig. 4, for the (110) surfaces of BX and BeY. Distances are in Å.

Surface	$\Delta_{1,\perp}$	$\Delta_{1,y}$	$\Delta_{2,y}$	$d_{12,\perp}$	$d_{23,\perp}$	d_{sb}	ω
BP(110)	0.423	0.937	1.091	1.119	1.441	1.895	24.4°
BAs(110)	0.485	0.992	1.161	1.177	1.524	2.007	26.1°
BSb(110)	0.549	1.102	1.421	1.284	1.674	2.224	26.5°
BeS(110)	0.466	0.942	1.997	1.332	1.717	1.999	26.3°
BeSe(110)	0.543	1.007	1.280	1.395	1.822	2.143	28.3°
BeTe(110)	0.614	1.118	1.391	1.515	1.977	2.350	28.8°

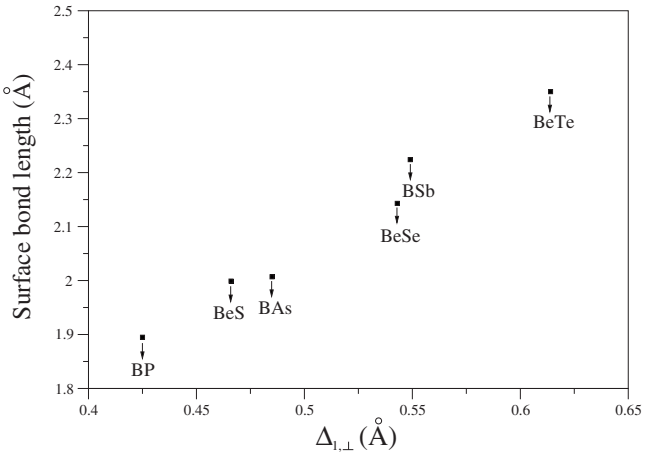

FIG. 5. Calculated equilibrium buckling $\Delta_{1,\perp}$ vs surface bond length for the (110) surfaces of BX and BeY compounds. The arrows are only used to point to the material labels.

along the zigzag chain direction are the A'' modes while atomic vibrations perpendicular to this direction are the A' mode at the $\bar{\Gamma}$ and $\overline{X'}$ points. A detailed comparison of the calculated surface phonon modes for BX(110) at the $\bar{\Gamma}$ point

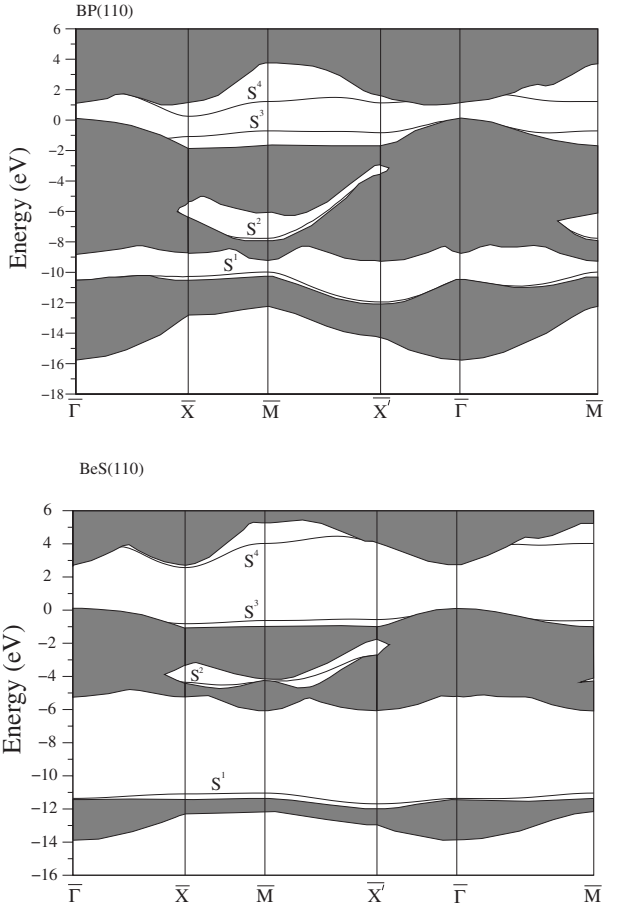

FIG. 6. The electronic band structures of the BP(110) and BeS(110) clean surfaces. The projected bulk spectrum is shown by hatched regions while localized occupied states are shown by thick curves and the localized unoccupied state is shown by the thin curves.

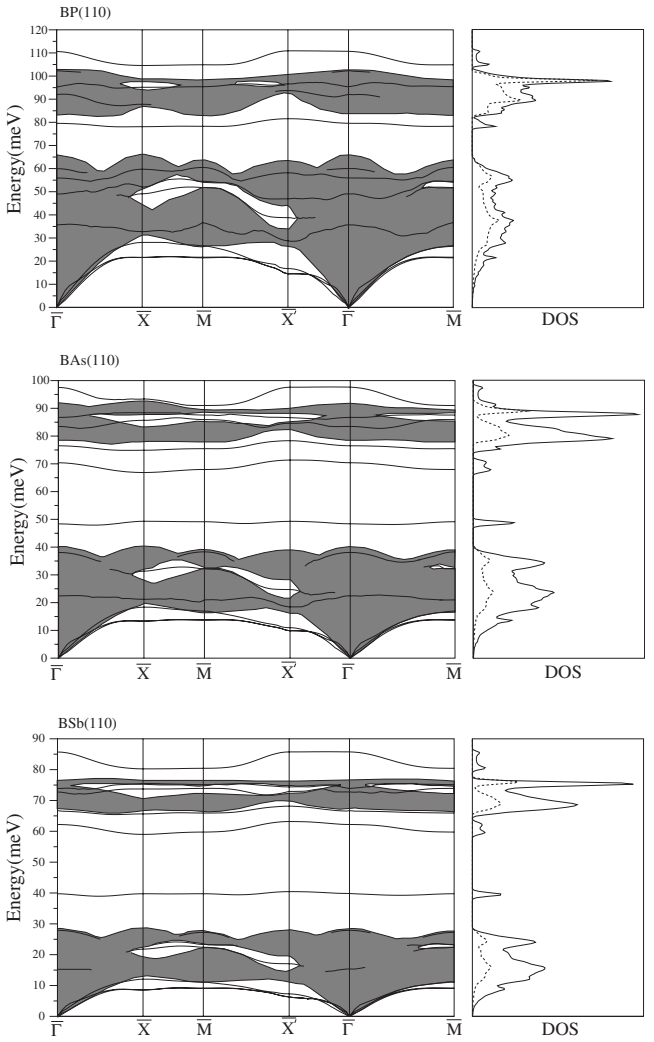

FIG. 7. Phonon-dispersion curves and density of phonon states of the BX(110) (X=P, As, and Sb) surfaces. For phonon-dispersion curves, the calculated results are shown by thick solid curves while bulk projected is shown by hatched region. For the density of phonon states, the solid curve is obtained from the (110) slab supercell calculation with the relaxed geometry, while the dotted curve shows the bulk density of states.

is presented in Table VI. This comparison is made according to the energy location and displacement characters of the phonon modes on these surfaces at the $\bar{\Gamma}$ point. It is important to note that the phonon modes, listed in this table, have similar displacement patterns and their energies are different from each other due to different reduced masses and lattice constants. The lowest optical surface phonon modes at the zone center are calculated at 35.65, 22.45, and 15.37 meV for BP(110), BAs(110), and BSb(110), respectively. This phonon mode is a cationic phonon mode which results from the opposing motion of top two layer cation atoms with components both in the [110] and [001] directions. We have also observed an anionic phonon mode with energies of 55.94, 48.38, and 39.77 meV for BP(110), BAs(110), and BSb(110), respectively. The first layer boron vibration is dominant in this phonon mode for all the BX(110) surfaces. We should note that this phonon mode lies in the acoustic-optical gap

TABLE VI. Calculated phonon frequencies (in meV) of BX(110) surfaces at the $\bar{\Gamma}$ point.

	A''			A'				
BP(110)	92.06	102.39	35.65	49.03	55.94	79.59	95.05	110.62
BAs(110)	76.51	86.73	22.45	38.09	48.38	70.40	83.49	97.53
BSb(110)	66.70	74.00	15.37	27.90	39.77	62.21	72.75	85.71

region for the (110) surface of BAs(110) and BSb(110) surfaces. The A' gap modes at 79.59 [BP(110)], 70.40 [BAs(110)], and 62.21 [BSb(110)] meV are localized on the second layer B atoms. In addition to these gap phonon modes, the vibrations of second layer B atoms generate the phonon modes at 95.05, 83.49, and 72.75 meV for the (110) surface of BP, BAs and BSb, respectively. The highest surface optical phonon mode for these surfaces results from the motion of first layer B atoms.

The surface acoustic modes are found as localized for large part of the surface Brillouin zone. An interesting point to note is that the surface acoustic modes are basically drawn out of the bulk acoustic modes, but drop in energy due to reduced coordination of surface atoms. At the zone edge of $\overline{X'}$ point, we have identified two surface acoustic phonon modes for all the BX(110) surfaces. The second acoustic mode is polarized in the saggital plane (with representation A') and thus contains components of the longitudinal and one of the transverse bulk acoustic branches. The first surface acoustic mode is polarized in the shear-horizontal plane (representation A'') and thus originates from the other transverse bulk acoustic branch. Only one phonon mode lies in the stomach gap region for all the BX(110) surfaces. This phonon mode is found at 38.81 meV for BP(110) and 24.73 meV for BAs(110) and 17.08 meV for BSb(110). For all the considered surfaces, this phonon mode comes from the vibrations of surface layer atoms. All gap phonon modes and the highest surface optical phonon mode at this **q** point have energies and displacement patterns similar to their counterparts at the zone center. As a result, our calculations predict similar optical phonon modes at the $\bar{\Gamma}$ and $\overline{X'}$ points because there is a mirror reflection symmetry when the wave vector is along the $\bar{\Gamma}$-$\overline{X'}$ direction.

Along the symmetry directions $\bar{\Gamma}$-$\bar{X}$ and $\bar{\Gamma}$-$\bar{M}$, surface phonon modes show a mixture of shear-horizontal and saggital-plane polarizations. The vibrational patterns of selected surface phonon modes for BSb(110) at the $\bar{X}$ point are plotted in Fig. 8. The lowest frequency of 8.54 meV corresponds to the vibrations of the first layer Sb and second layer B atoms with components in both the [110] and [001] directions. On the whole this pattern has more SP polarization than SH polarization. A similar observation has been made for the (110) surface of BP and BAs. The energy of second acoustic mode is found to be 12.07 meV for the BSb(110) surface. This phonon mode has 56% SH character with large atomic vibrations from the first layer Sb atoms. This phonon mode has 57% SH character for BAs(110) and 56% SH character for BP(110). We have identified only one phonon mode in the stomach gap region for all the BX(110) surfaces. The energy of this phonon mode is 21.81 meV for BSb(110), 31.36 meV for BAs(110), and 49.11 meV for BP(110). It is interesting to note that this phonon mode includes large atomic vibrations from first layer anion atoms along the zigzag chain direction. The phonon mode at 39.76 meV in Fig. 8 is a true localized surface-phonon mode with 62% SP polarization. The similar phonon mode has been found at 49.31 meV for BAs(110) with same polarization character. The second gap phonon mode on BSb(110) with an energy of 59.0 meV is localized on the second layer cation atoms. The corresponding phonon mode for BAs(110) has been observed at 66.88 meV which also includes large atomic vibrations from the second layer cation atoms. The third gap phonon mode for BSb(110) lies very close to the optic bulk phonon edge. The energy of this phonon mode at the $\bar{X}$ point is 65.63 meV with 67% SP polarization. A similar phonon mode has been found at 74.91 meV for BAs(110) and 78.10 meV for BP(110). We have found only one surface optical gap phonon mode at the optical-optical gap region with energy of 73.72 meV for BSb(110), 85.69 meV for BAs(110), and 95.10 meV for BP(110) surface. Along the $\bar{\Gamma}$-$\bar{X}$ direction, we have observed a dispersive branch for the highest surface optical phonons. The zone boundary energy at this phonon mode at the $\bar{X}$ point is 80.26 meV. The corresponding phonon mode for BAs(110) and BP(110) has been found at 92.08 and 104.57 meV, respectively. For all the considered surfaces, this phonon mode has 60% SP character.

The calculated surface phonon dispersion curves and density of states for BeS(110), BeSe(110), and BeTe(110) are shown in Fig. 9. Two phonon branches lie above the bulk optical continuum. This feature is different from other II-VI(110) surfaces. The higher one shows dispersion along the several symmetry directions, except $\bar{\Gamma}$-$\overline{X'}$ direction. There is a large gap between the acoustical and optical phonons in the bulk which results from the large mass difference between cation and anion atoms. There are up to two localized phonon branches in this gap region for all three surfaces. For the BeSe(110) and BeTe(110) surfaces, we find no appreciable change in the dispersion of the first gap phonon mode while there is a noticeable amount of dispersion for the second gap phonon mode. The first gap phonon mode gives rise to a clear peak in the phonon density of states between the bulk acoustic and optical-phonon regions for the (110) surface of BeSe and BeTe. For BeS(110), there is no clear peak in the phonon density of states due to gap phonon modes. The reason for this is that gap phonon modes on this surfaces lie below the optic bulk phonon edge or just above the edge of the bulk acoustic bands.

Some of the frequencies for all three surfaces at $\bar{\Gamma}$ and $\overline{X'}$ are listed in Table VII. In the text, we only discuss zone-center surface phonon modes. The lowest optical phonon

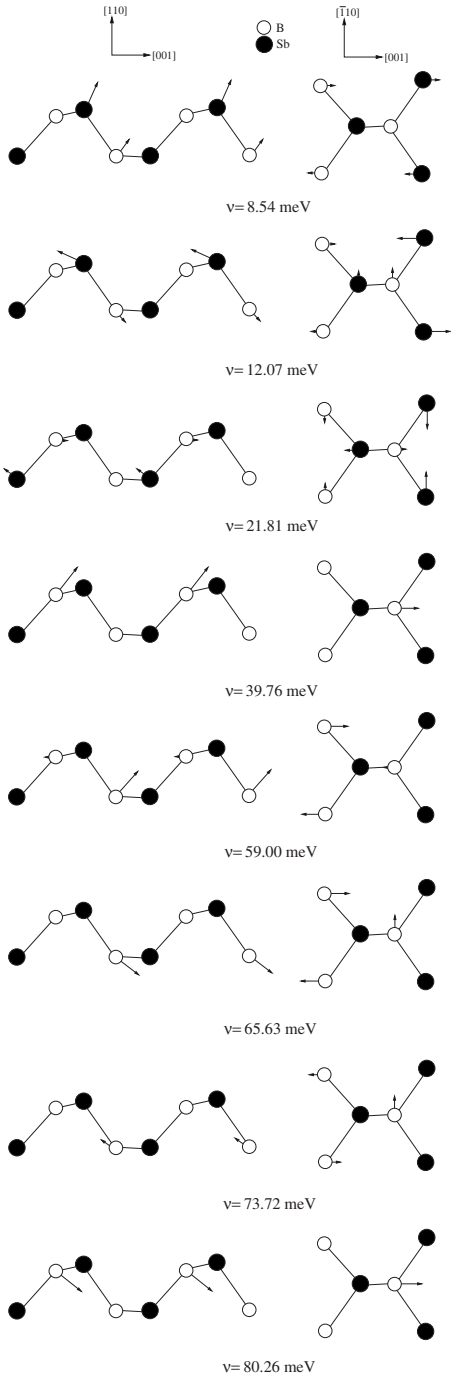

FIG. 8. The vibrational patterns of selected surface phonon modes for BSb(110) at the $\bar{X}$ point.

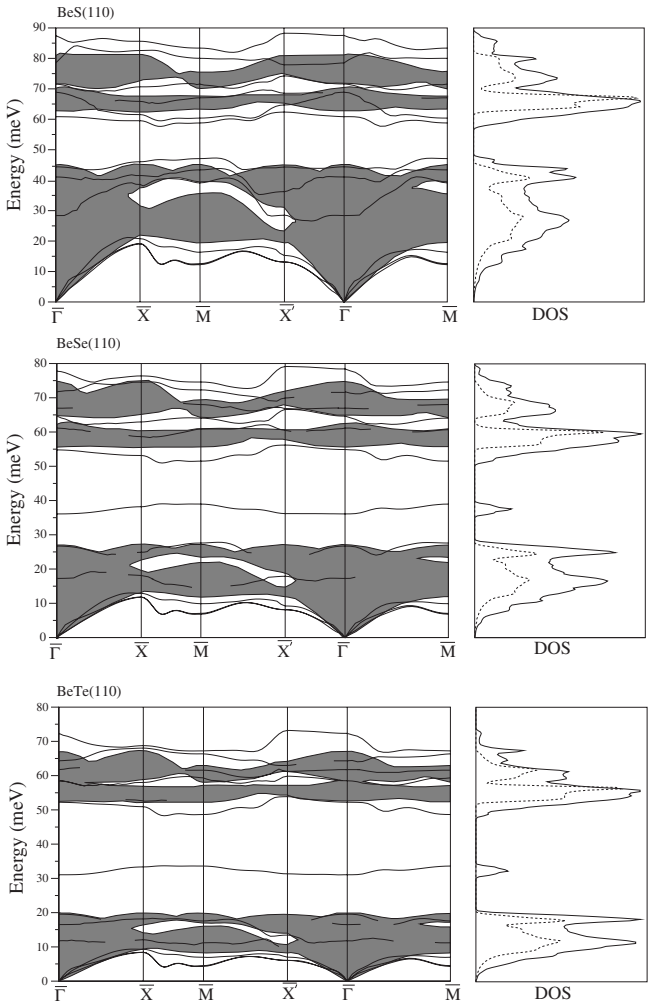

FIG. 9. Phonon-dispersion curves and density of phonon states of the BeY(110) (Y=S, Se, and Te) surfaces. For phonon-dispersion curves, the calculated results are shown by thick solid curves while bulk projected is shown by hatched region. For the density of phonon states, the solid curve is obtained from the (110) slab supercell calculation with the relaxed geometry, while the dotted curve shows the bulk density of states.

mode for all three surfaces has A' character with energies of 28.33 meV for BeS(110), 17.26 meV for BeSe(110), and 11.80 meV for BeTe(110). This phonon mode is characterized by opposing motion of first and second layer anion atoms in the surface normal direction. The lower gap phonon mode for BeSe(110) and BeTe(110) comes from the vibrations of the first layer cation atoms with components in both the [110] and [001] directions. The zone-center energies of this phonon mode are found to be 36.09 for BeSe(110) and 31.07 for BeTe(110). The analysis of zone-center surface phonon modes indicate that BeS(110) shows different dynamical behavior from other two surfaces. We associate this difference with smaller cation and anion mass difference in BeS(110). For this surface, we have observed a rotational phonon mode at 41.06 meV with opposing motion of surface layer atoms in the surface normal direction. Another interesting phonon mode at 44.38 meV on this surface is a bond-stretching character which comes from the opposing motion of surface layer atoms in the [001] direction. These phonon modes, not listed in Table VII, have not been observed for the (110) surface of BeSe and BeTe. The vibrations of second layer Be atoms creates gap phonon modes with energies of 60.90 meV for BeS(110), 54.78 meV for BeSe(110) and 52.24 meV for BeTe(110). The higher energy phonon modes are also localized on the Be atoms due to light mass of Be atom. In particular, the highest surface optical phonon mode includes large atomic vibrations from first layer Be atoms with components along [001] as well as along the surface normal direction. This picture is different from other II-

TABLE VII. Calculated phonon frequencies (in meV) of BeY(110) surfaces at the $\bar{\Gamma}$ and $\overline{X'}$ points.

	A''				A'		
At $\bar{\Gamma}$ point							
BeS(110)	68.97	78.56	28.33		60.90	71.62	86.40
BeSe(110)	67.03	71.75	17.26	36.09	54.78	64.66	77.75
BeTe(110)	61.76	64.33	11.80	31.07	52.24	58.51	72.35
At $\overline{X'}$ point							
BeS(110)	15.28	77.89	13.12		62.36	74.26	88.25
BeSe(110)	9.21	66.79	8.11	36.19	56.19	66.65	79.13
BeTe(110)	7.00	61.24	6.05	31.33	53.86	62.97	73.18

VI(110) surfaces [ZnS(110), ZnTe(110), and CdTe(110)].[36] For these surfaces, there are large atomic vibrations from third layer atoms for the corresponding phonon mode. This difference may be due to very small mass of Be atom because a similar observation has been made for BX(110) and BN(110) surfaces.

Table VIII gives calculated surface frequencies and their polarization characters for selected phonon modes on the BeY(110) surfaces at the $\bar{M}$ point. The lowest frequency in this table is a Rayleigh mode and mainly corresponds to the motion of the first layer anion atoms with components in both the surface normal and [001] directions. Thus, this phonon mode is mainly polarized in the saggital plane for all three surfaces. The phonon mode at 16.31 meV on BeS(110) has 40% SP character with opposing vibrations of first layer anion and second layer cation atoms in the [001] direction. For this phonon mode, the first layer cation and second layer anion atoms vibrate in the zigzag chain direction. A similar phonon mode has been observed at 9.89 meV for BeSe(110) and 6.98 meV for BeTe(110). At this **q** point, two gap phonon modes are found in the bulk acoustic-optical gap region for all three surfaces. The energies of these phonon modes are 47.08 and 58.79 meV for BeS(110) surface. These phonon modes are localized on the first layer and second layer Be atoms, respectively. Two phonon modes lie above the bulk continuum for all three surfaces. The lower one for all three surfaces includes atomic vibrations from the first layer Be atoms with components in both surface normal and [001] directions. The second one is dominated by the vibrations of first layer Be atoms in the zigzag chain direction.

4. Comparison of surface phonon modes

In this section first, the calculated phonon results for the BX(110) surfaces will be compared with each other in detail. We find that the surface relaxation is similar for all three surfaces. Thus, the difference in their phonon energies can be explained in terms of the reduced mass and total mass differences. In order to support our idea, in Fig. 10, we have plotted the Rayleigh wave frequency at the $\bar{X}$ point against the square root of the inverse total mass of the surface cation and anion. We have observed a linear behavior between the Rayleigh wave frequency and the square root of the inverse total mass of the surface cation and anion. In addition to this observation, we have found that the gap phonon modes of BAs(110) and BSb(110) surfaces can be related to each other according to lattice constant and reduced mass difference. Finally, the highest surface optical phonon mode shows a similar dispersion for all three surfaces. Moreover, the energy of this phonon mode is plotted against the reduced mass of cation and anion atoms at the $\bar{X}$ point in Fig. 10. Due to this linear behavior, one can say that the effective force constant for this mode on all three surfaces is very similar. Above observations has been made for the BeY(110) surfaces.

Different from III-V(110) surfaces,[33–35] the highest surface optical branch for the BX(110) surface shows a dispersion along the $\bar{\Gamma}$-$\bar{X}$ direction. However, this branch is a

TABLE VIII. Selected phonon frequencies (in meV) of BeY(110) surfaces at the $\bar{M}$ point.

Material	Energies					
BeS(110)	12.26	16.31	47.08	58.79	80.03	83.38
USP	94	40	71	35	82	78
USH	6	60	29	65	18	22
BeSe(110)	6.82	9.89	38.97	51.50	68.01	74.60
USP	92	42	70	25	75	77
USH	8	58	30	75	25	23
BeTe(110)	4.33	6.98	33.61	48.64	61.59	67.23
USP	91	42	70	22	74	78
USH	9	58	30	78	26	22

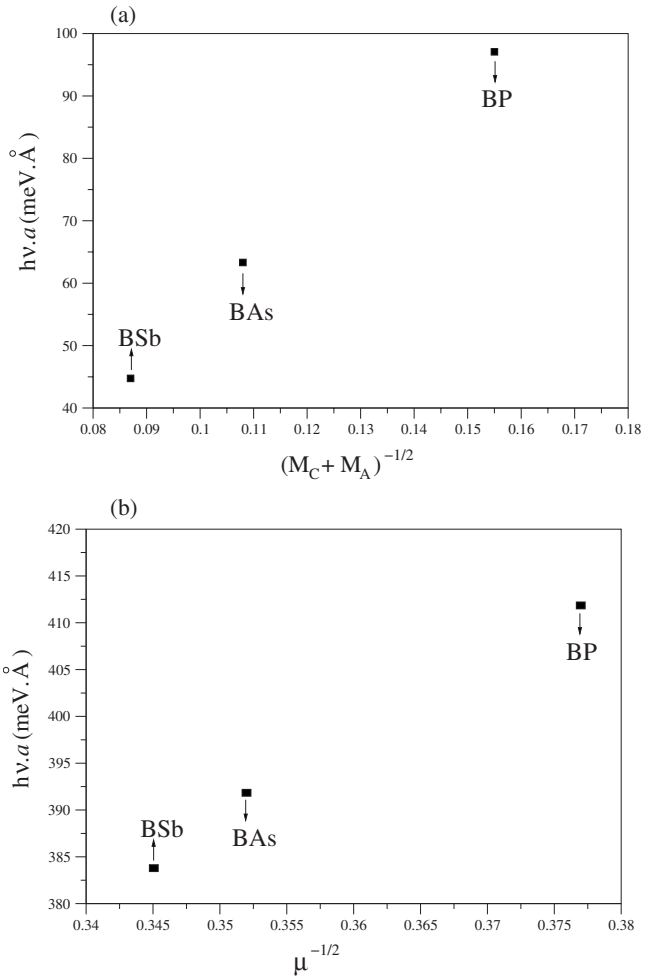

FIG. 10. (a) The Rayleigh wave frequency against the square root of the inverse total mass of the surface cation and anion and (b) the energy of the highest surface optical phonon mode against the reduced mass of cation and anion atoms at the $\bar{X}$ point. The arrows are only used to point to the material labels.

nearly flat for the AlSb(110) and GaSb(110) surfaces for which $m_{\text{anion}} > m_{\text{cation}}$. Thus, this difference can be connected with a very small mass of B atom. It is interesting to note that a similar observation has been made between the BeY(110) and other II-VI(110) surfaces.[36] Atomic displacement pattern of this branch is dominated by the vibrations of B (Be) atoms for the BX(110) [BeY(110)] surfaces. On the other hand, our previous studies indicated that this phonon mode includes large atomic vibrations even third layer cation atoms for the (110) surface of AlSb and GaSb. Only two acoustical phonon modes have been identified along $\bar{\Gamma}$-$\bar{X}'$ for the BX(110) surfaces while previous studies indicated three acoustic phonon modes for other III-V(110)[33–35] surface along this symmetry direction. Moreover, the lowest of them has A'' character for the BX(110) surfaces while it is of A' mode for other III-V(110) surfaces.[33–35] It has been observed that localized gap surface phonon modes lie just above the edge of the bulk acoustic bands and below the optic bulk phonon edge for the AlSb(110) surface for which $m_{\text{anion}} > m_{\text{cation}}$. Although the mass of anion atom is much larger than the mass of cation atom for BSb(110) surfaces, we have observed that localized gap phonon branches are well separated from bulk phonons for BSb(110) surface. These differences can be related to the smaller ionicity of BSb. Finally, the rotational and bond-stretching phonon modes have been only identified for the (110) surface of BeS.

IV. SUMMARY

In this study, we have presented a complete theoretical analysis of the structural, elastic, electronic, and vibrational properties of BX (X=P, As, Sb) and BeY (Y=S, Se, Te) semiconductors by employing a first-principles scheme, based on the application of the plane-wave pseudopotential method within the density-functional theory and linear response method. The calculated elastic results for both group materials are in good agreement with available experimental and theoretical results. From results of the electronic properties of BX, we have confirmed that these materials are indirect band gap. We have also presented the phonon spectra and density of states for BP, BAs, and BSb semiconductors. Some trends in their dynamical properties have been established. In particular, the calculated zone-center phonon modes for BP are in good agreement with experimental observations. After presenting bulk properties of BX and BeY, we have applied an *ab initio* pseudopotential density-functional theory to study structural, electronic, and dynamical properties of the BX(110) and BeY(110) surfaces. In general, the atomic relaxation parameters on these surfaces show a pattern similar to that obtained for other III-V(110) and II-VI(110) surfaces. We have also identified surface electronic states on the BX(110) and BeY(110) surfaces by presenting their surface electronic structures together with their projected bulk electronic structures. The phonon dispersion curves for BX(110) [BeY(110)] are compared with each other in detail. This comparison shows that the effective force constants for surface optical phonon modes on all the considered surfaces are very similar and differences in their energy locations can be related to the reduced masses and lattice constants differences. Moreover, we have compared surface phonon modes on BX(110) [BeY(110)] surfaces with the corresponding phonon modes on the III-V(110) [II-VI(110)] surfaces. Because of very small cation mass, the BX(110) [BeY(110)] surfaces are found to show somewhat different dynamical behavior than the III-V(110) [II-VI(110)] surfaces. These differences can be summarized as follows. First, the atomic displacement pattern of the highest phonon mode on BX(110) [BeY(110)] has a different polarization characteristic from its analog on III-V(110) [II-VI(110)] surfaces. Second, this phonon mode is well separated from the bulk optical phonon bands for BX(110) surfaces while this phonon branch lies very close to the bulk optical phonon bands for the III-V(110) surfaces. Third, we have observed only two acoustic phonon modes at the $\bar{X}'$ point for BX(110) surfaces while three acoustic phonon mode are found for other III-V(110) surfaces at this **q** point.

ACKNOWLEDGMENTS

This work was supported by the Scientific and Technical Research Council of Turkey (TUBITAK).

[1] Ch. Verie, in *Proceedings of the International Conference on Heteroepitaxy Growth, Characterization and Device Applications*, edited by B. Gill and R.-L. Aulombaud (World Scientific, Singapore, 1995), p. 73.
[2] A. Waag, F. Fischer, H. J. Lugauer, T. Litz, J. Laubender, U. Lunz, U. Zhender, W. Ossau, T. Gerhardt, M. Moller, and G. Landhehr, J. Appl. Phys. **80**, 792 (1996).
[3] M. P. Surh, S. G. Louie, and M. L. Cohen, Phys. Rev. B **43**, 9126 (1991).
[4] P. Rodriguez-Hernandez, M. Gonzalez-Diaz, and A. Munoz, Phys. Rev. B **51**, 14705 (1995).
[5] M. Gonzalez-Diaz, P. Rodriguez-Hernandez, and A. Munoz, Phys. Rev. B **55**, 14043 (1997).
[6] M. Ferhat, B. Bouhafs, A. Zaoui, and H. Aourag, J. Phys.: Condens. Matter **10**, 7995 (1998).
[7] M. Ferhat, A. Zaoui, M. Certier, and H. Aourag, Physica B **252**, 229 (1998).
[8] B. Bouhafs, H. Aourag, M. Ferhat, and M. Certier, J. Phys.: Condens. Matter **12**, 5655 (2000).
[9] G. L. W. Hart and A. Zunger, Phys. Rev. B **62**, 13522 (2000).
[10] N. Benosman, N. Amrane, S. Mecabih, and H. Aourag, Physica B **304**, 214 (2001).
[11] S. Q. Wang and H. Q. Ye, Phys. Status Solidi B **240**, 45 (2003)
[12] H. Meradji, S. Drablia, S. Ghemid, H. Belkhir, B. Bouhafs, and A. Tadjer, Phys. Status Solidi B **241**, 2881 (2004).
[13] N. Chimot, J. Even, H. Folliot, and S. Loualiche, Physica B **364**, 263 (2005).
[14] D. Madouri and M. Ferhat, Phys. Status Solidi B **242**, 2856 (2005).
[15] A. Zaoui, S. Kacimi, A. Yakoubi, B. Abbar, and B. Bouhafs, Physica B **367**, 195 (2005).
[16] D. Heciri, L. Beldi, S. Drablia, H. Meradji, N. E. Derradji, H. Belkhir, and B. Bouhafs, Comput. Mater. Sci. **38**, 609 (2007).
[17] S. Azzi, A. Zaoui, and M. Ferhat, Solid State Commun. **144**, 245 (2007).
[18] *Numerical Data and Functional Relationships in Science and Technology, Physics of Group IV Elements and III-V Compounds*, Landolt-Börnstein, New Series, Group III Vol. 17, Pt. A, edited by O. Madelung (Springer-Verlag, Berlin, 1982).
[19] W. Wettling and J. Windscheif, Solid State Commun. **50**, 33 (1984).
[20] C. C. Wang, M. Cardona, and A. G. Fisher, RCA Rev. **25**, 159 (1964).
[21] A. Fomichev, I. I. Zhukova, and I. K. Polushina, J. Phys. Chem. Solids **29**, 1025 (1968).
[22] I. Lyakhovskaya, T. M. Zimkina, and V. A. Fomichev, Fiz. Tverd. Tela (Leningrad) **12**, 174 (1970).
[23] S. Dalui, S. N. Das, S. Hussain, D. Paramanik, S. Verma, and A. K. Pal, J. Cryst. Growth **305**, 149 (2007).
[24] J. A. Sanjurjo, E. Lopez-Cruz, P. Vogl, and M. Cardona, Phys. Rev. B **28**, 4579 (1983).
[25] G. P. Srivastava, H. M. Tütüncü, and N. Günhan, Phys. Rev. B **70**, 085206 (2004).
[26] H. W. L. Alves and K. Kunc, J. Phys.: Condens. Matter **4**, 6603 (1992).
[27] D. N. Talwar, G. Thaler, S. Zaranek, K. Peterson, S. Linger, D. Walker, and K. Holliday, Phys. Rev. B **55**, 11293 (1997).
[28] L. Huang, X. Wang, and B. Ao, J. Phys.: Condens. Matter **16**, 7829 (2004).
[29] D. Touat, M. Ferhat, and A. Zaoui, J. Phys.: Condens. Matter **18**, 3647 (2006).
[30] R. Pässler, J. Appl. Phys. **101**, 093513 (2007).
[31] K. Bouamama, P. Djemia, N. Lebga, and K. Kassali, High Press. Res. **27**, 269 (2007).
[32] Jose Luiz A. Alves, J. Hebenstreit, and M. Scheffler, Phys. Rev. B **44**, 6188 (1991).
[33] H. M. Tütüncü and G. P. Srivastava, Phys. Rev. B **53**, 15675 (1996).
[34] H. M. Tütüncü and G. P. Srivastava, Phys. Rev. B **59**, 4925 (1999).
[35] J. Fritsch and U. Schrder, Phys. Rep. **309**, 209 (1999).
[36] H. M. Tütüncü, R. Miotto, and G. P. Srivastava, Phys. Rev. B **62**, 15797 (2000).
[37] D. M. Ceperley and B. J. Alder, Phys. Rev. Lett. **45**, 566 (1980).
[38] J. P. Perdew and A. Zunger, Phys. Rev. B **23**, 5048 (1981).
[39] R. Stumpf, X. Gonge, and M. Scheffler, *A List of Separable, Norm-Conserving, Ab Initio Pseudopotentials* (Fritz-Haber-Institut, Berlin, 1990).
[40] W. Kohn and L. J. Sham, Phys. Rev. **140**, A1133 (1965).
[41] M. J. Mehl, J. E. Osburn, D. A. Papaconstantopoulos, and B. M. Klein, Phys. Rev. B **41**, 10311 (1990).
[42] P. Söderlind, O. Eriksson, J. M. Wills, and A. M. Boring, Phys. Rev. B **48**, 5844 (1993).
[43] S. Baroni, S. de Gironcoli, A. Dal Corso, and P. Giannozzi, Rev. Mod. Phys. **73**, 515 (2001); http://www.pwscf.org
[44] F. D. Murnaghan, Proc. Natl. Acad. Sci. U.S.A. **50**, 697 (1944).
[45] H. M. Tütüncü, Ph.D. thesis, University of Exeter, United Kingdom, 1998.